JGR Atmospheres

Key Points:
- Losses of nitrous oxide (N_2O) and chlorofluorocarbon ($CFCl_3$) are modulated ($\pm 5\%$ amplitude) by the Quasi-Biennial Oscillation
- Stratospheric air depleted in N_2O and $CFCl_3$ is transported down to the surface where it affects the observed surface variability
- The seasonal cycle of surface N_2O in the northern hemisphere is driven mostly by stratospheric loss rather than surface emissions

Correspondence to:
D. J. Ruiz,
djruiz@uci.edu

How Atmospheric Chemistry and Transport Drive Surface Variability of N_2O and CFC-11

Daniel J. Ruiz[1] , Michael J. Prather[1] , Susan E. Strahan[2] , Rona L. Thompson[3] , Lucien Froidevaux[4] , and Stephen D. Steenrod[2]

[1]Department of Earth System Science, University of California, Irvine, CA, USA, [2]NASA, Goddard Space Flight Center, Greenbelt, MA, USA, [3]Norwegian Institute for Air Research, Kjeller, Norway, [4]NASA, Jet Propulsion Laboratory, California Institute of Technology, Pasadena, CA, USA

Abstract Nitrous oxide (N_2O) is a long-lived greenhouse gas that affects atmospheric chemistry and climate. In this work, we use satellite measurements of N_2O, ozone (O_3), and temperature from the Aura Microwave Limb Sounder (MLS) instrument to calculate stratospheric loss of N_2O, and thus its atmospheric lifetime. Using three chemistry transport models simulating the Aura period 2005–2017, we verify the stratospheric sink using MLS data and follow that loss signal down to the surface and compare with surface observations. Stratospheric loss has a strong seasonal cycle and is further modulated by the Quasi-Biennial Oscillation (QBO); these cycles are seen equally in both observations and the models. When filtered for interannual variability, the modeled surface signal is QBO-caused, and it reproduces the observed pattern, highlighting the potential role of the QBO in tropospheric chemistry and composition, as well as in model evaluation. The observed annual surface signal in the northern hemisphere matches well with the models run without emissions, indicating the annual cycle is driven mostly by stratosphere-troposphere exchange (STE) flux of N_2O-depleted air and not surface N_2O emissions. In the southern hemisphere (SH), all three models disagree and thus provide no guidance, except for indicating that modeling annual STE in the SH remains a major model uncertainty. Parallel model simulations of $CFCl_3$, which has greater stratospheric loss that N_2O and possibly surreptitious emissions, show that its interannual variations parallel those of N_2O, and thus the observed N_2O variability can identify the stratospheric component of the observed $CFCl_3$ variability.

Plain Language Summary Nitrous oxide (N_2O) is a long-lived greenhouse gas that drives climate change and ozone depletion, posing a threat to society's health and well-being. The abundance of N_2O at Earth's surface, where we can measure it most precisely, fluctuates over seasons and years due to increasing human emissions, variable natural emissions, varying stratospheric destruction, and the movement of air throughout the atmosphere. Scientists use these fluctuations to separate natural from human emissions and quantify what humans can do to reduce the growth in N_2O. In this work, we model the physical side of atmospheric N_2O that drives fluctuations through chemistry and atmospheric transport. Our model simulations match most of the observed seasonal and multi-year fluctuations seen in satellite and surface observations, indicating that N_2O loss is causing the dominating signal, not emissions. Unfortunately, in the southern hemisphere, the annual cycle of the models is in disagreement and cannot help us interpret the observed fluctuations. In addition to helping understand the human role in N_2O increases, we find that the N_2O observations provide a valuable test of models and guidance to improve them.

1. Introduction

Nitrous oxide (N_2O) is a long-lived greenhouse gas that directly affects climate and participates in stratospheric ozone depletion, further altering atmospheric composition and posing a threat to human health and society. Agricultural practices and fossil fuel combustion have played important roles in increasing the global burden of fixed nitrogen (Erisman et al., 2013), leading to a steady increase in atmospheric N_2O abundance over the last 50 years (Fowler et al., 2015; Hall et al., 2007; Thompson, Chevallier, et al., 2014; Tian et al., 2020). The photochemical sink of N_2O is almost entirely stratospheric and is manifested at the surface as a negative perturbation in N_2O abundance (Hamilton & Fan, 2000; Mahlman et al., 1986; Nevison et al., 2004). Uncertainty in this stratospheric influence confounds the scientific effort to derive the

location and magnitude of surface emissions and to identify anthropogenic sources from the variability in surface abundance (Nevison et al., 2004, 2011, 2018; Thompson, Chevallier, et al., 2014; Thompson, Ishijima, et al., 2014; Thompson, Patra, et al., 2014; Tian et al., 2018). These N_2O source-inversion studies seeking to accurately derive emissions must be able to model and remove the stratospheric variability from the surface fluctuations (Corazza et al., 2010; Ray et al., 2020; Thompson et al., 2011). The most extensive of such studies (Thompson, Chevallier, et al., 2014; Thompson, Ishijima, et al., 2014) continues to admit "errors in stratosphere–troposphere exchange (STE) represent an important source of model error." Here, we use a much wider range of stratospheric and surface measurements, along with models specific to the years of observation and provide a more critical evaluation of the stratospheric influence on surface N_2O.

This work uses three independent chemistry transport models (CTMs) that calculate N_2O stratospheric loss and compares them with the loss calculated directly from NASA's Aura Microwave Limb Sounder (MLS) satellite observations using a photochemical box model as in Prather et al. (2015). We design new tracer simulations that allow us to follow the signal of stratospheric loss down to the surface. We examine the National Oceanic and Atmospheric Administration (NOAA) Earth System Research Laboratories (ESRL) surface N_2O measurements for stratospheric-driven variability. The observed latitude-by-month annual patterns could be caused by either emissions or the stratospheric sink; whereas the Quasi-Biennial Oscillation (QBO) pattern seen in the measurements appears to be uniquely stratospheric (see IPCC AR5, WG1, Chapter 6, Figure 6.19; Ciais et al., 2013). The QBO alternates phase about every 28 months (Baldwin et al., 2001) and increases (decreases) the N_2O sink by enhancing (suppressing) tropical upwelling of N_2O-rich air to the loss region in the tropical middle stratosphere (Strahan et al., 2015). The QBO can also modulate the transport of N_2O-depleted air to the surface. This work identifies a distinct QBO signal originating from the stratosphere that appears in both observed and modeled surface N_2O. These results are a 20-year follow-on to the Hamilton and Fan (2000) original work that showed a QBO-forced signal in surface N_2O but lacked the satellite data, surface observations, and modern CTM capabilities to confirm it. If we use the QBO signal as a metric to test a CTM's stratosphere-troposphere exchange (STE), we can constrain the larger annual surface pattern that is also of stratospheric origin.

$CFCl_3$ (CFC-11), another ozone depleting substance, has a stratospheric photochemical loss region much lower at ~25 km altitude compared to the N_2O loss region at ~32 km, and thus the phasing and amplitude of stratospherically depleted air at the surface could be different from that of N_2O. Given the recent fugitive emissions of CFC-11 (Montzka et al., 2018; Rigby et al., 2019), we also included some CFC-11 simulations in parallel with N_2O. Since there are no equivalent MLS-like observations for CFC-11 to integrate loss (and lifetimes), we rely solely on model results to investigate stratosphere-to-surface variability as in Ray et al. (2020).

In Section 2, we present the updated N_2O lifetime based on the 2005–2018 MLS observations and three independent CTMs driven with meteorology of the same period. In spite of some biases in absolute magnitude, the models are able to capture most of the observed variability of stratospheric N_2O loss throughout the period. In Section 3, we follow the stratospheric loss of N_2O and CFC-11 down to the surface, focusing on the long-term annually smoothed statistics that separate surface variability tied to the QBO from seasonal cycles in transport and surface emissions. The three models each use a different meteorology to drive the atmospheric circulation, but they all predict a clear QBO signal similar to that in the NOAA surface data. The larger annual cycle driven by seasonality of emissions and transport including stratospheric influence has previously been studied by Nevison et al. (2004). Section 4 looks at the modeled annual cycle in surface N_2O driven only by stratospheric loss. The comparison with observations is limited here, as we did not model surface emissions, and we rely on comparisons with the more extensive study of the annual N_2O cycle by Nevison et al. (2004). We conclude in Section 5 with a discussion of how this work can provide an innovative model-measurement STE test.

The overall goal of developing more accurate quantification of STE here is to derive a best estimate of the signal of stratospheric N_2O-depleted air at the surface. With this knowledge, we can more accurately determine the signal of the emissions in the surface observations leading to more accurate emission estimates through inverse modeling.

2. Observed and Modeled Stratospheric Loss

### 2.1. The MLS Record of N₂O Loss

Since mid-2004, the MLS instrument aboard the Earth Observing System Aura satellite has provided reliable measurements of trace gases throughout the stratosphere and upper troposphere. Employing the method established in Prather et al. (2015) (henceforth P2015), we adopt MLS profiles and expand the calculation of N_2O loss from 2005–2010 to 2005–2018. This work uses coincident monthly mean profiles of N_2O, O_3, and temperature that are zonally averaged and available at every latitude in 5° bins (87.5°N–87.5°S), similar to the data record from Global OZone Chemistry And Related trace gas Data for the Stratosphere (GOZCARDS; Froidevaux et al., 2015) but on a finer latitude grid. N_2O loss in TgN/yr is calculated for each month-latitude cell using these three profiles. In P2015, we used MLS observations from the 640 GHz (N_2O) channel, which failed in mid-2013 and have since been replaced by the 190 GHz channel. The profiles for temperature and O_3 use the same measurement channels as in P2015 but are derived from updated (version 4; V4) retrieval algorithms. After 2009, N_2O values in the equatorial stratosphere show a drift of approximately −0.75%/yr at the 68 hPa layer (see Froidevaux et al., 2019; Livesey et al., 2018). N_2O loss is centered on the middle stratosphere (∼10 hPa) and sensitivity tests show the effect of the drift at lower profiles on calculated N_2O loss is small: +1% in N_2O at 68 hPa increases total loss by +0.020%; and +1% at 46 hPa increases loss by +0.036%. Thus, a drift at 68 hPa of −6.75% from 2009 to 2018 would decrease the loss by 0.14% (0.018 TgN/yr). The drift at 46 hPa over the period is much smaller, −0.25%, and thus the effect on N_2O loss is negligible (<0.002 TgN/yr). In addition to the drift, there is an offset between the two N_2O channels due to possible systemic errors in MLS: N_2O-190 is biased 5%–10% high relative to N_2O-640 at 68 hPa and by <5% high at 46 hPa. Combining the maximum difference (10% and 5%), we calculate N_2O loss is +0.38% (0.05 TgN/yr) greater for N_2O-190. At the time of this work, release of version 5 (V5) MLS products began. Development of V5 sought to address the persistent bias between the two N_2O channels, but this is taken into account in our analysis and does not affect our results (Livesey et al., 2020). Overall, these errors are much smaller than the annual cycle or long-term variations, and their effect on the lifetime calculations is well below the uncertainty estimated for the lifetime (below).

Following the P2015 methodology, we use an offline photochemical column model to calculate photolysis rates and $O(^1D)$ densities from the MLS profiles, providing the loss of N_2O throughout the column. Solar cycle variability in photolysis rates is not included in these calculations, but an estimate of photolysis changes is discussed in Section 2.4. N_2O loss is calculated for each monthly profile and latitude bin from August 2004 through December 2018. The seasonal pattern of N_2O loss is matched very well by the CTMs (see P2015). Here, we focus on interannual variations using a 12-month running filter, and hence we present results centered on February 1, 2005 through July 1, 2018.

Over this period, the tropospheric mean abundance of N_2O increased almost linearly from about 319 ppb (nanomoles per mole) to 330 ppb, or equivalently from a burden of 1,528 to 1,586 TgN (using a scaling factor of 4.79 TgN/ppb [Prather et al., 2012; Volk et al., 1997]). We want to analyze a stationary time series, and so we rescale both the burden and chemical loss each month with the same factor so that the burden corresponds to our reference value of 320 ppb. With this scaling, the average N_2O loss over the MLS period 2005–2018 is 12.9 (interannual min-max ± 0.3) TgN/yr, corresponding to a global mean loss frequency of about 0.84%/yr.

Figure 1 compares our rescaled N_2O loss derived from past and current MLS products (different retrieval channels and version algorithms). The mean difference between V3 (P2015; green) and V4 products for the old N_2O (640 GHz; blue) channel is 2%, while the mean difference between V3 640 GHz (P2015; green) and the new updated V4 190 GHz channel (red) is much smaller during the overlapping period (2005–2010). This disagreement is well within the MLS uncertainty range in N_2O of 3%–5% (one-sigma). Interannual variability clearly shows a QBO signal and is nearly identical across the three records, except when the 640 GHz channel fails in the 2nd half of 2012. In the tropical lower-stratosphere, the downward propagating zonal winds of the QBO alternate direction every ∼28 months. The shear produced by descending winds can enhance or suppress transport of N_2O to the middle stratosphere where it is destroyed (∼10 hPa), and thus generate a QBO signal in the loss of N_2O.
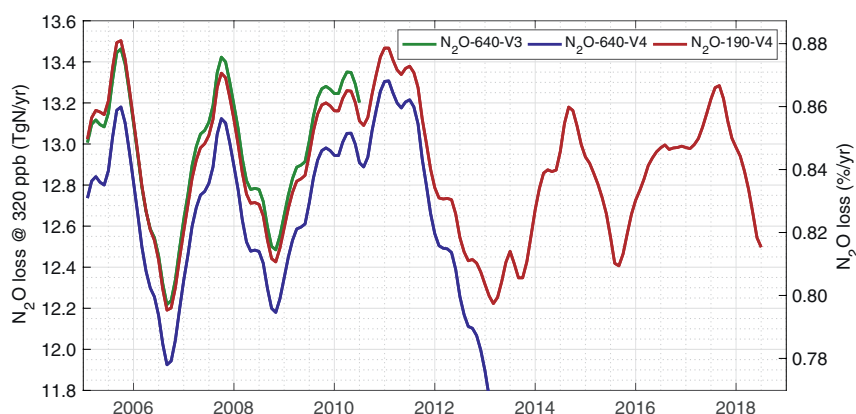
Figure 1. Rescaled loss of N_2O (TgN/yr, monthly values averaged over 12 months) calculated from Aura MLS measurements of N_2O, O_3, and temperature. The green line represents N_2O loss calculated with the version 3 (V3) N_2O product using the 640 GHz channel (data used in Prather et al., 2015). The blue line represents N_2O loss based on version 4 (V4), also at 640 GHz. The red line represents N_2O loss based on V4 at 190 GHz (primary data used here). The right *y*-axis shows the loss frequency (%/yr) of the total fixed burden when scaled to 320 ppb or 1,533 TgN. The O_3 profiles use the 240 GHz channel, and temperature uses 118 GHz (16–90 km) and 239 GHz (9–16 km). MLS, Microwave Limb Sounder; N_2O, nitrous oxide; V3, version 3; V4, version 4.

2.2. Chemistry-Transport Modeling of N_2O – Methods

For models, we identified three CTMs that could simulate stratospheric loss of N_2O using prescribed historical meteorology for the MLS period, see Table 1: the Goddard Space Flight Center (GSFC) Global Modeling Initiative (GMI) CTM, the Laboratoire de Météorologie Dynamique, Zoom, Version 5 (LMDz5) CTM, and the University of California Irvine (UCI) CTM. The CTMs are similar in resolution (1°–3° horizontal) with 40–70 atmospheric layers. GMI uses Modern-Era Retrospective analysis for Research and Applications-2 (MERRA-2) wind fields and full stratosphere-troposphere chemistry (Strahan et al., 2016); LMDz5 uses the European Center for Medium-Range Weather Forecasts Re-Analysis-Interim (ECMWF ERA-Interim) meteorology with prescribed fields for $O(^1D)$ and photolysis rates from a previous run (Remaud et al., 2018); and UCI uses ECMWF Integrated Forecast System (IFS) pieced forecasts with a linearized stratospheric chemistry including O_3, N_2O, and CH_4 (Hsu & Prather, 2010; Prather et al., 2017).

We design a CTM simulation whereby any variability in N_2O in the stratosphere down to the surface will be driven completely by stratospheric loss and atmospheric transport. If emissions are used to maintain the observed N_2O, then the surface variability will also be determined by the location and magnitude of those emissions, confounding the stratospheric signal. Resetting lower-boundary N_2O to observations does not get around this constraint since it is effectively a surface source. To isolate the stratospheric N_2O signal, the CTMs simulate an artificial tracer N2OX like that in Hamilton and Fan (2000). N2OX is initialized as N_2O at the beginning of the simulations, has the same stratospheric chemical loss frequency as N_2O, has no sources or emissions, and thus decays at a semi-regular rate of about 0.8%/yr (see Figure 1 for loss frequency and supplementary Figure S1a for change in burden (TgN) of N_2O versus N2OX). With the decaying N2OX

Table 1
Participating Models

Model name	Meteorology	Resolution	years	Reference
GSFC GMI CTM	MERRA-2	1°; 72 layers	1980–2018	Strahan et al. (2016)
LMDz5 CTM	ERA Interim	1.25° × 3.75°; 39 layers	1995–2016	Thompson et al. (2014)
UCI CTM	ECMWF IFS Cy38r1	1.1°; 57 layers	1990–2017	Prather et al. (2017)

Abbreviations: CTM, chemistry transport model; ECMF, European Center for Medium-Range Weather Forecasts; ERA, ECMF Re-Analysis; GMI, Global Modeling Initiative; GSFC, Goddard Space Flight Center; IFS, Integrated Forecast System; LMDz, Laboratoire de Météorologie Dynamique; MERRA-2, Modern-Era Retrospective analysis for Research and Applications-2.

tracer, the loss frequency (%/yr) values are calculated directly from the model loss divided by the model burden, averaging both the loss and burden over 12 months (i.e., 12-month running mean). For comparison with absolute amounts such as mass loss frequency (TgN/yr) or surface fluctuations in ppb, we scale the model-derived chemical loss to a mean tropospheric abundance of 320 ppb (our reference standard established in Section 2.1).

The relative atmospheric distribution of N$_2$O will be different between N2OX (driven only by a stratospheric sink) and real (observed) N$_2$O (driven by surface emissions and a stratospheric sink). N2OX is a pure decay mode tracer (lifetime is a true e-fold; see Prather, 1998), whereas loss of N$_2$O is kept at steady state due to emissions. This results in N2OX having a greater stratospheric abundance and greater stratospheric loss by about 2% when compared to a surface-driven N$_2$O with the same mean tropospheric abundance. For example, in the UCI model with a surface source maintaining a 320 ppb N$_2$O abundance, the lifetime is 139 years; but for the no-source decaying N2OX, it is 135 years. As a bias offset, this difference is much less than the uncertainty in the MLS derived lifetime and also less than the model-to-model differences. As an added complication, the observed atmospheric N$_2$O is not in steady state but is increasing at about 0.25%/yr, and thus, for the same stratospheric abundance and loss, the tropospheric burden is larger than when run at steady state. This effect is <1% (i.e., a 4-year lag from troposphere to mid-stratosphere) and also well within the uncertainties here.

Solar-cycle variations in ultraviolet (UV) flux along with ensuing photochemical changes in O$_3$ are included in GMI and (obviously) in the observations, but not in LMDz5 or UCI. The change in N$_2$O loss from solar minimum to maximum is buffered: increased UV flux at 190–240 nm will drive greater N$_2$O loss, but also greater upper-stratospheric O$_3$ columns that reduce N$_2$O photolysis. Overall, the O$_3$ increases vary from 0% to 3%, and the UV flux changes near 200–210 nm (peak N$_2$O loss region) is estimated to be 2%–6% (Ball et al., 2019; Gray et al., 2010; Hood, 2004). We judge the uncertainty in solar-cycle and solar-rotation effects for this study to be well within the MLS observational uncertainties (~2% level) or the model differences.

2.3. Chemistry-Transport Modeling of N$_2$O Loss

The modeled N2OX mean loss frequencies (%/yr) are compared with MLS N$_2$O in Figure 2a and summarized in Table 2. For the MLS period (2005–2018), UCI mean loss frequency is about 0.10%/yr less than MLS, while LMDz5 is 0.04%/yr greater, and GMI is a match. In P2015, both GMI and UCI had similar offsets from MLS, but the new GMI model matches MLS. The GMI chemistry has not changed much, but the P2015 GMI was run with MERRA Goddard Earth Observing System, Version 5 (GEOS-5) circulation, while the current GMI uses MERRA-2 circulation. Based on P2015 (their Figure 3), these different loss rates are not caused by differences in photochemistry between the GMI simulations, but rather the circulation's ability to maintain high levels of N$_2$O at 10 hPa in the tropics where most of the loss occurs. It is interesting that LMDz5 and UCI have the largest difference since both models are using ECMWF meteorology, but in different forms (ERA-Interim vs. IFS cycle38r1 forecasts). If we drop all the model values by 0.02%/yr to account for bias of N2OX loss versus a surface forced N$_2$O (see example with UCI CTM; Section 2.2 and Table 2), then MLS falls in between LMDz5 and GMI with UCI still having the largest underestimate of loss rate at any given time.

Comparing the QBO-like variability in N$_2$O loss across the models with the MLS-derived loss, we find that all have about the same peak-to-peak amplitude, ±0.04%/yr (Figure 2a). Unusually, the UCI model, with the largest bias in total loss (see above), has the closest direct match to the MLS variations (correlation coefficient, cc = 0.86); while for GMI (cc = 0.45) and LMDz5 (cc = 0.32), the variations occur at different times. In 2013, GMI shows an extra peak loss (i.e., due to enhanced upwelling) that is not seen in the other models or observations, which may account for the lower correlation. For the 15-year period before MLS (1990–2004), the models show a similar overall range of variability, but less temporal correlation between them than in the MLS period. LMDz5 and UCI are reasonably consistent showing parallel variations over 1995–2005 (cc = 0.64), but GMI (with LMDz5 cc = 0.33 and with UCI cc = 0.41) clearly diverges.

For the pre-MLS period, the models show less agreement with one another than in the MLS period and also exhibit significant shifts in their loss frequencies. N2OX loss in GMI starts at 11.5 TgN/yr, rising to >13 TgN/yr over this pre-MLS period; whereas UCI loss also starts at 11.5 TgN/yr but returns to that value by 2004. We conclude that large differences emerge from 1990 to 2004 in the circulation of the tropical
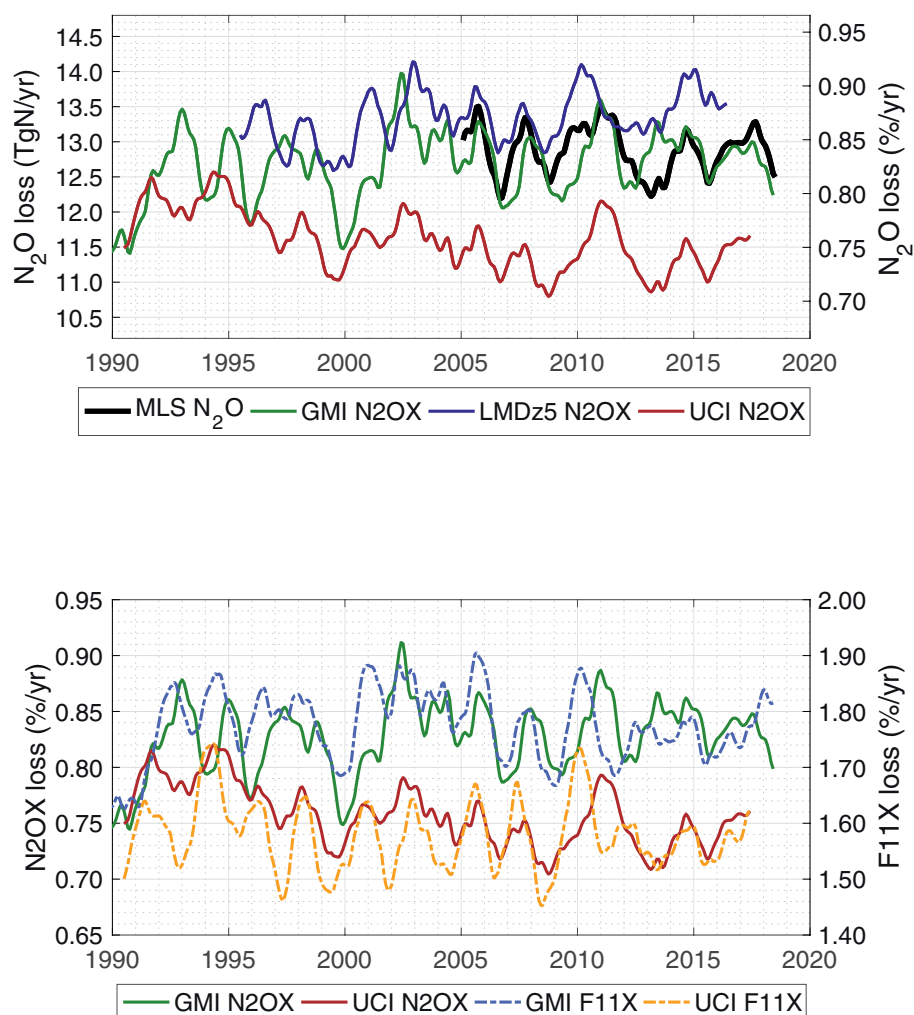
Figure 2. (a) Absolute loss of N$_2$O (TgN/yr; left axis) and global mean loss frequency (%/yr, right axis) for MLS observations (2005–2018, thick black line, GMI [1990–2018, green]), LMDz5 (1995–2016, blue), UCI (1990–2017, red). Absolute loss for the models with decaying tracer N2OX is scaled to a tropospheric mean of 320 ppb. MLS loss frequency is based on NOAA's tropospheric burden rescaled to 320 ppb. (b) Modeled loss (%/yr) of N2OX (solid lines; left y-axis) and F11X (dashed lines; right y-axis). Results are shown for GMI (green, blue) and UCI (red, gold). Note: F11X loss y-axis scale is twice that of N2OX loss. GMI, Global Modeling Initiative; LMDz, Laboratoire de Météorologie Dynamique; MLS, Microwave Limb Sounder; N$_2$O, Nitrous oxide; NOAA, National Oceanic and Atmospheric Administration; UCI, University of California Irvine.

middle stratosphere between ECMWF (both ERA-Interim and IFS Forecasts used in LMDz5 and UCI, respectively) and MERRA-2 (GMI), and that these differences are maintained consistently throughout the MLS period. These disagreements may stem from known transport problems in the MERRA-2 subtropical lower stratospheric circulation (Coy et al., 2016; Manney et al., 2017) that also affects upwelling rates to the tropical middle stratosphere where N$_2$O is destroyed. In addition, Douglass et al. (2017) showed that the MERRA-2 transport circulation had time-dependent biases prior to the Aura MLS period that caused poor agreement with simulated long-lived trace gases. Stauffer et al. (2019) showed that changes in the observing system in 1998 led to significant improvements in the MERRA-2 stratospheric circulation.

2.4. Decadal Trends and Variability in N$_2$O Lifetime

The lifetimes of the gases in Table 2 are simply the inverse of their global mean loss frequencies, shown for the MLS period (2005–2018, ending in 2016 for LMDz5 and 2017 for UCI) and for the pre-MLS period (1990–2004, beginning in 1995 for LMDz5). The full MLS record of 12-month averages runs from February

Table 2

Annual Mean Loss Frequency (%/yr) and Respective Lifetime (yr) of N_2O, N2OX, and F11X in Each of the Simulations for the MLS Overlap Period (2005–2018) and for the Previous Years of Each Simulation (Years Vary)

	1990–2004		2005–2018	
	Loss (%/yr)	Lifetime (yr)	Loss (%/yr)	Lifetime (yr)
MLS N_2O	-	-	0.84	119
GMI N2OX	0.82	122	0.83	120
LMDz5 N2OX	0.86	116	0.88	114
UCI N2OX	0.77	130	0.74	135
UCI N_2O @ 320 ppb	0.75	133	0.72	139
GMI F11X	1.79	56	1.77	57
UCI F11X	1.58	63	1.58	63

MLS N_2O uses NOAA ESRL N_2O burden for 2005–2018. Aura MLS overlap period may end slightly prior to December 2018 depending on the CTM. LMDz5 reports only for 1995–2016; and UCI, for 1990–2017. GMI is the only model to report an earlier decade 1980–1990, which has reduced mean loss frequencies for N2OX (0.74%/yr) and F11X (1.60%/yr), similar to UCI; but the stratospheric transport in GMI for that period is discredited (Douglass et al., 2017).

Abbreviations: GMI, Global Modeling Initiative; LMDz, Laboratoire de Météorologie Dynamique; MLS, Microwave Limb Sounder; N_2O, Nitrous oxide; UCI, University of California Irvine.

1, 2005 to July 1, 2018 and has a mean loss frequency of 0.84%/yr, corresponding to a lifetime of 119 years. This lifetime is only slightly longer than the 117 years (118 years when rescaled to 320 ppb) reported in P2015 for the period 2005–2010. The three models show different decadal shifts in N_2O lifetime over the extended period: UCI has a clear long-term increase (i.e., decreasing N_2O loss); LMDz5 has a small decrease; and GMI has almost no trend but oscillates widely (20% min-to-max amplitude) in the pre-MLS period. GMI is the only model to report an earlier decade, which was proven to be unreliable prior to ~2000 due to unrealistic transport of air-parcels in the middle stratosphere (Douglass et al., 2017).

Many studies find long-term shifts in the annual Brewer-Dobson circulation (BDC) which transports tropospheric air to the stratosphere (Butchart, 2014). As climate change drives the acceleration of the BDC, one would expect increased loss of F11 and N_2O. Fu et al. (2019) finds changes to the BDC over the last four decades based on satellite observations and reanalysis data. However, we do not see trends in N_2O lifetime over the sustained climate change of the MLS period (2005–2018). Only GMI shows shifts in lifetime during the early years of the simulation (1980–2000), but these are discredited as noted above.

What changes in the chemistry could drive interannual or decadal shifts in lifetime? N_2O loss is driven primarily by the overhead O_3 column that controls photolysis rates (90% of loss), and secondarily by local O_3 that is the source of $O(^1D)$ oxidation (10% of loss). For the MLS period, there is a positive trend in upper stratospheric O_3 of 1%–2% per decade above 30 km (see WMO, 2018, Chapter 3, Figures 3–8; Braesicke et al., 2018). This O_3 increase shields N_2O loss, increasing the lifetime, and it is naturally included in the loss rate derived from MLS observations. Given an effective optical depth of about 1 for the O_3 column above 30 km, we might expect N_2O photolysis to respond with similar percentage reductions. The MLS loss in Figure 2 shows much larger variability (10%) but is consistent with a 1%–2% drop (~0.2 TgN/yr) in loss rate. The LMDz5 and UCI models used parameterized N_2O loss not including chlorine changes, but the GMI model used full chemistry that did. A simple linear trend fit shows that MLS and UCI agree in overall trend, while LMDz5 and GMI are different, but we find little statistical significance in these differences given the short length of the record.

Solar cycle variations in the UV-flux change N_2O photolysis directly, in addition to changing O_3. The solar-cycle driven O_3 changes in the upper stratosphere are small over the MLS period, estimated to be +1% during the weak maximum of Cycle 24 in 2011–2015 (WMO 2018, Figures 3–7). This has a small impact, but UV-flux driven increase in N_2O loss is estimated to be a 4%–7% at full solar maximum (P2015's Table 2). Since the recent Cycle 24 had less than half the amplitude of typical cycles, we estimate that N_2O loss may have increased by about 0.3 TgN/yr. This solar cycle was not included in LMDz5 and UCI but was in GMI. The MLS loss, calculated with the offline UCI photochemistry box model, also did not include this direct solar cycle effect although it would have included the ozone changes noted above (see P2015). It is possible that the anomalous 2013 peak loss in GMI of magnitude 0.6 TgN/yr may be in part a solar cycle signal.

2.5. Chemistry-Transport Modeling of CFC-11 – Methods

Using only GMI and UCI CTMs, we simulate a synthetic F11X tracer that has the loss frequency of $CFCl_3$ and decays without sources (see supplementary Figure S1b). LMDz5 did not simulate F11X. With no equivalent stratospheric observational counterpart, we cannot compare the modeled stratospheric loss with observations. F11X responds to stratospheric circulation changes in the lower stratosphere with loss occurring in the tropics about 8 km below that of N_2O. Although N_2O must be transported through the lower stratosphere into the middle stratosphere where it is destroyed, it is not particularly sensitive to the rate of tropical upwelling below 24 km because little N_2O is lost there. Thus, the covariance of F11X and N2OX losses identifies some coherence in tropical upwelling in the stratosphere from 20 to 40 km altitude. In addition, F11X
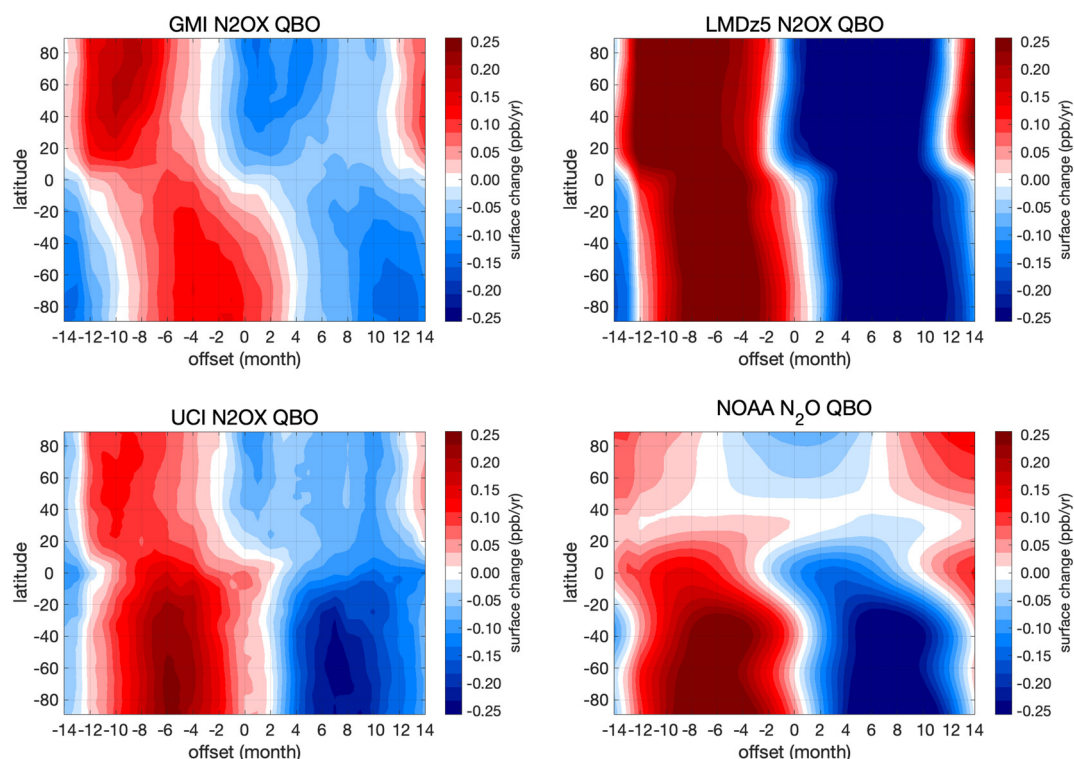
Figure 3. Surface N₂O change (ppb/yr) composites centered on the QBO phase transition at 40 hPa based on a rescaled tropospheric abundance of 320 ppb. Composites show the mean QBO surface impact throughout the overlap period (years 2001–2016*; six standard QBO cycles) for each respective data set. Simulations (top panel and bottom left) are of N2OX (zero emissions), while the NOAA ESRL observations (bottom right) are of surface N₂O (with emissions). Warmer colors indicate positive change changes with respect to a tropospheric mean abundance of 320 ppb (i.e., driven by lower loss frequencies, resulting in greater abundances of N2OX) while cooler colors coincide with increases in loss rates (see Figure 2). *Note: the 2010/11 anomalous QBO centered on August 2010 has been removed from these composites and is shown separately in Figure S4. ESRL, Earth System Research Laboratories; N₂O, Nitrous oxide; NOAA, National Oceanic and Atmospheric Administration; QBO, Quasi-Biennial Oscillation.

can indicate if the surface signal of chemically depleted stratospheric tracers depends on the loss region (e.g., ~24 km for F11X and ~32 km for N2OX).

2.6. Chemistry-Transport Modeling of CFC-11 Loss and Lifetime

UCI and GMI F11X mean loss frequencies (%/yr; Figure 2b) and lifetimes (Table 2) are compared with each other and N2OX. The behavior of the N2OX and F11X losses are similar, but not identical: for GMI the cc of N2OX versus F11X is 0.38 for years 2001–2016; and for UCI, it is 0.37 (see Table S2). For both models, the F11X mean loss frequency and amplitude is about twice that of N2OX. This increased loss frequency puts the lifetime of UCI F11X during the MLS overlap period at 63 years, which is slightly longer than GMI's at 57 years. The timing of most F11X extrema matches well across the two models (cc = 0.47 for GMI vs. UCI F11X) and is comparable with their N2OX counterparts, indicating transport variations in the lower strato-sphere are similar between MERRA-2 and ECMWF-IFS. The systematic difference in N2OX loss frequency between UCI and GMI carries over to F11X in proportion to the mean loss frequency. Thus, the systematic UCI-GMI difference in annual mean tropical upwelling is consistent throughout the stratosphere. The most obvious N2OX-F11X disagreement occurs in 2010, with the F11X peak loss reached nearly a full year before the corresponding N2OX peak loss. Interestingly, the timing of this F11X peak in GMI and UCI agree with the timing of the early portion of the broad MLS N₂O peak loss (Figure 2a) during an anomalous QBO (see Section 3.3). Another notable N2OX-F11X mismatch occurs in 2013 but only for GMI. In addition to not being captured by the other models and the MLS observations, the anomalous peak loss of N2OX in GMI (see Section 2.4) was also not accompanied by F11X peak loss. Since tropical transport directly affects the

loss rates, the low correlation between N2OX and F11X in the two models indicates that upwelling changes phase with altitude. When including pre-MLS years (1990–2005), there are no obvious decadal shifts in F11X loss rate, unlike N2OX.

3. Surface Impacts of Stratospheric QBO

3.1. Introduction and Methods

The Brewer-Dobson overturning circulation transports air masses throughout the stratosphere (Butchart, 2014), bringing air containing tropospheric levels of N_2O and $CFCl_3$ upward in the tropics to their respective loss regions where they are photolyzed or destroyed by $O(^1D)$. Then, air that is photochemically depleted in these gases is transported down to the lower stratosphere outside the tropics where STE carries N_2O- and $CFCl_3$-depleted air into the troposphere and down to the surface. The overturning circulation, including the stratosphere-to-troposphere flux, has a large seasonal cycle driven by solar heating, but also well-known interannual variability associated with dynamics like the tropical QBO and wintertime sudden stratospheric warmings.

The surface signal in these model calculations should be uniquely stratospheric since we included no tropospheric chemistry or emissions for N2OX and F11X. The N_2O loss due to O^1D in the troposphere, 1% of the budget (Hsu & Prather, 2010), is not included here. Therefore, the observed surface QBO signal provides an unambiguous test of STE of N_2O-depleted air on sub-decadal time scales. We compare modeled N2OX with NOAA ESRL surface observations of N_2O (Dlugokencky et al., 2019) over years 2001–2016.

Surface N_2O measurements from NOAA are taken from the cooperative global air sampling network collected by the Global Greenhouse Gas Reference Network for the Carbon Cycle and Greenhouse Gases (CCGG) Group. These air-flask samples are collected weekly from a discrete and dense network of global background sites, air-sampling towers, small aircraft, and cooperative regional background sites (Dlugokencky et al., 2019). The rate of change over a 12-month period is calculated to remove seasonal trends and produce zonally averaged annual growth rates of N_2O (ppb/yr) for each month.

For this QBO analysis, we calculate the modeled interannual (year-to-year) rate of change for each month (e.g., the %/yr change in January 1991 = N2OX$_{Jan1991}$/N2OX$_{Jan\ 1990}$−1), while the observed change is based on the annual growth rate of N_2O. As expected, the long-term mean interannual rate of change for modeled N2OX matches the model's loss frequency (Table 1, −0.76% to −0.89%/yr) and is opposite in sign to that for real N_2O with its observed growth rate for this period of +0.25%/yr. In supplementary Figure S2, we show the latitude-by-month interannual anomalies with the mean removed for the full period available. The N2OX anomalies from the three models look remarkably like the observed N_2O, although they may be more regular than the observations. The observations will, of course, also include interannual variability in emissions that is not QBO-related, but to first order, it appears that the majority of interannual variability in observed N_2O is QBO-driven as shown in Ray et al. (2020). The interannual change (%/yr) can be converted to abundance (ppb/yr) through multiplying by 320 ppb, and fluctuations are about ±0.7 ppb, equivalent to the annual growth rate. The mean annual cycle has a slightly larger amplitude and is discussed in Section 4.

For a clearer picture of the QBO signal at the surface, we create a composite of QBO cycles in surface N_2O in ppb/yr by averaging at each latitude for each month starting 14 months prior and extending to 14 months after the QBO (Figure 3). For this diagnostic, the mean interannual percent change is removed and we multiply models and observations by 320 ppb. The synchronization point for each QBO cycle is chosen as the month when the zonal wind at 40 hPa shifts from westerly (negative) to easterly (positive) based on the Singapore sonde data (Newman, 2020). If we extend these graphs beyond ±14 months, the coherent signal of the QBO is lost. Since the NOAA ESRL data begins in 2001 and LMDz5 extends only to 2016, this work is restricted to these years for consistency. This period includes 7 QBO phase transitions (01/2002, 03/2004, 04/2006, 04/2008, 08/2010, 04/2013, 07/2015). The QBO period centered on 08/2010 is clearly anomalous: there was a disruption to the stratospheric QBO, there was a strong La Niña, and the NOAA surface QBO composite was highly anomalous, unlike the models (see supplementary Figure S4). Therefore, our composites use only the standard six QBO cycles and we address the anomalous 2010 QBO in Section 3.3.

The Ray et al. (2020) study showed QBO impacts at the surface for CFC-11 and N_2O, using a chemistry-climate model that was tied to the historical meteorology only by nudged winds in the tropical stratosphere. Therefore, the lowermost stratospheric circulation, jet streams, and stratosphere-troposphere exchange, and tropospheric mixing were mostly driven by climatological sea-surface temperature boundary conditions, unlike the CTMs meteorologies used here that followed the synoptic weather conditions of the period. Their paper focuses on CFC-11, and the published diagnostics for modeled N_2O (global mean surface) cannot be readily incorporated in this analysis.

3.2. QBO Impact

Composites of the six standard QBOs for surface N_2O/N2OX in Figure 3 show a distinct pattern and general agreement among the models and the NOAA ESRL observations, indicating that this QBO-composite is robust. Variability caused by emissions tied to wildfires or El Niño-Southern Oscillation (ENSO) events would only degrade this NOAA composite. All four data sets look similar in terms of timing and latitudinal patterns before and after the QBO phase transition, especially in the southern hemisphere (SH). The negative N_2O anomaly occurs first in the southern hemisphere (NH) in the ~2 months leading up to the phase change and extends into the SH 0–4 months afterward. This pattern cannot simply be the lagged interhemispheric transport of a NH signal because the SH amplitude is greater than or equal to that in the NH. The surface variability for UCI ($\sigma = 0.03$%/yr), GMI ($\sigma = 0.03$%/yr), and NOAA observations ($\sigma = 0.04$%/yr) are all comparable, however, LMDz5 variability is twice as large ($\sigma = 0.08$%/yr). For LMDz5 and GMI, the amplitudes in each hemisphere are similar, but for UCI and NOAA, the amplitude is much greater in the SH than in the NH. This larger SH amplitude of QBO-modulated signal was expected for the UCI CTM as it is also seen in stratosphere-to-troposphere ozone flux (Hsu & Prather, 2009). UCI performs the best among the CTMs at capturing the observed pattern overall (correlation coefficient, cc, of UCI vs. NOAA is 0.80). All the models do well in the SH: cc is 0.93 for LMDz5, 0.89 for UCI, 0.70 for GMI. In the NH, the models are distinctly worse: 0.54 for LMDz5, 0.51 for GMI, and 0.32 for UCI. The models tend to agree with each other in the NH QBO composite (except for LMDz5 having twice the amplitude), and thus the disagreement with the observations may be caused by the predominantly NH emissions and their annual cycle disrupting the QBO composite. These results are part of the Taylor statistics (standard deviation, root-mean-square error, and correlation coefficients) for the models versus observations (NOAA) given in supplementary Table S1. In terms of phasing between the hemispheres, GMI has the best NH-SH phase shift, keeping opposite signs in the hemispheres, while LMDz5 and UCI (both using ECMWF products) have much less phase shift between hemispheres. The observed NH-SH difference in amplitude is only matched by UCI, indicating that LMDz5's meteorological fields have distinctly different STE fluxes, at least in the NH over a QBO cycle.

With GMI and UCI also running tracer F11X, we assemble similar diagnostics for surface F11X and find surprising results (see supplementary Figure S3 and Table S2). The surface patterns for F11X match those of their N2OX counterparts nearly exactly but with twice the amplitude. The cc values of F11X versus N2OX within each model range from 0.96 to 1.00 for the annual, QBO composite, or the 2010 anomalous QBO at the surface. This is surprising since the stratospheric losses have cc values of 0.37–0.38. The implication is that the large QBO signal in the chemical creation of N_2O-depleted (or F11-depleted) air in the tropical stratosphere is not transmitted to the surface. Rather, it is the QBO-related changes in dynamics of the mid-latitude lowermost stratosphere that causes the surface signal. The large QBO signal in tropical N_2O loss is mixed and forgotten by the time it reaches the lowermost stratosphere.

3.3. Anomalous QBOs and ENSO-Related Emissions

Not all QBOs are alike and the composite smooths over these differences. During the 2005–2018 MLS period, there were two notably anomalous QBOs. In 2010/11, the QBO pattern was disrupted with a weakening, but not reversal of the zonal westerly winds, followed by a strengthening (Coy et al., 2017; Newman, 2020). This pattern appears as a deep and persistent westerly phase that results in prolonged, enhanced tropical upwelling in the mid-stratosphere (Newman et al., 2016; Osprey et al., 2016). A stronger disruption occurred in 2015/16, causing a QBO phase reversal where the westerlies changed to descending easterlies. Following the 2015/16 disruption, there was a long westerly phase until mid-2018. A primary consequence of the QBO cycle is to alter upwelling of trace gases to loss regions in the stratosphere, and anomalous QBOs

should be manifested in the stratospheric loss of N_2O and F11 (Tg/yr). In Figure 1, we find a fairly regular (~28 months) signal in the MLS-derived loss, but in 2010/11 the peak loss from enhanced upwelling during the westerly phase is sustained for more than a year. None of the CTMs are able to capture this sustained peak loss: GMI and UCI N2OX simulations show peak loss near the end of this period; while the LMDz5 N2OX simulations have peak loss near the beginning (Figure 2). For this 2010/11 anomaly, the modeled F11X peak loss (GMI and UCI only) occurs about 1 year prior to the N2OX peak loss, which then coincides with minimum F11X loss. Because F11 is destroyed much lower in the stratosphere than N_2O, this pattern indicates that the enhanced tropical upwelling in the two regions is disconnected and starts in the lower stratosphere. There are other periods when the F11X and N2OX losses are uncorrelated, but the 2010/11 period is unique in that both models show the same pattern. In sharp contrast, the 2015/16 QBO anomaly in MLS N_2O loss is well matched in both GMI and UCI simulations, and further, the F11X losses parallel those of N_2O. The sustained westerlies during 2016/18 produce a broad peak of N_2O loss that is well matched by GMI and UCI. The UCI simulation ended during this anomaly but appears to capture the first half of the peak loss. GMI was able to capture this anomaly in its entirety, but unfortunately, the LMDz5 simulation ended before the anomaly began.

The next question is how these anomalous QBOs are manifested as anomalies in surface abundance (ppb/yr). For this, we compare the anomalous 2010/11 QBO centered at the 08/2010 QBO phase change (supplementary Figure S4), with the composites of six standard QBO cycles (Figure 3). The NOAA surface pattern of this 2010 anomaly is surprisingly different from its composite with a large positive N_2O anomaly in the SH from about −9 to +4 months (relative to the QBO phase change), which extends into a weaker NH positive anomaly centered about 0 to +9 months (see Figure S4). This anomaly is also captured by the separate NOAA Halocarbon and other Atmospheric Trace Species group (HATS; not shown here) using a separate surface observing network, and thus this pattern is most likely a robust global signal. In sharp contrast, the modeled patterns mostly match their standard-QBO composites despite minor differences (i.e., reversal from negative to positive in the SH for GMI).

Thus, for more than a year, N_2O showed a sustained growth of 0.25 ppb/yr above the long-term average (about 0.8 ppb/yr over the period analyzed here). This growth was not caused by a reduction in stratospheric influx of N_2O-depleted air that we modeled. The simplest explanation is that starting in late 2009, there was an enhanced N_2O source of about 1 TgN that accumulated in the SH and then mixed into the NH with the typical interhemispheric exchange time of about 1 year. This source could be from the equatorial Pacific Ocean because the inter-tropical convergence zone is north of the equator and the emissions would accumulate in the SH.

The 2010/11 anomalous QBO was accompanied by the cool phase (La Niña) of ENSO, while the 2015/16 anomalous QBO was accompanied by a strong warm phase (El Niño). Studies have shown that El Niño events, which suppress tropical upwelling in the Eastern Pacific, lead to a reduction in oceanic N_2O emissions; while the opposite is true for La Niña events (e.g., Butler et al., 1989; Cline et al., 1987; Ji et al., 2019). Nevison et al. (2007) and Thompson et al. (2019) show that the ENSO index is negatively correlated with N_2O abundance and growth rates. This supports our simplistic proposal above that an equatorial source of ~1 TgN during the 2010 La Niña can explain the observed anomaly.

We have a unique capability here in that we have three independent CTMs generating N_2O surface patterns that include all the chemistry and transport, but without emissions. The dynamical link between the QBO and ENSO is unclear (Coy et al., 2017) and poorly reproduced in models (Serva et al., 2020). Nevertheless, we expect our CTM simulations based on reanalysis meteorological fields should include a semblance of the chemistry and transport variability, QBO and ENSO related, that affects surface N_2O. Thus, we remove the modeled chemistry-transport-driven surface variability from the observed signal (i.e., NOAA observations minus models from Figure S2) to search for an emissions signal tied to ENSO. Since the obvious QBO amplitude of this signal is different across the models (Figure 3), we rescale the models' surface variability to match the root-mean-square deviation from the mean of the observed QBO signal (Figure 3) before calculating the residuals. The NOAA-minus-model residuals are then correlated with the Niño 3.4 index (calculated from the monthly Extended Reconstructed Sea Surface Temperature, Version 5 by NOAA's Climate Prediction Center) at each latitude. Figure 4 shows that this presumably emissions-driven anomaly is negatively correlated with the Niño 3.4 index (opposite in sign to the 2010 La Niña anomalies as expected)
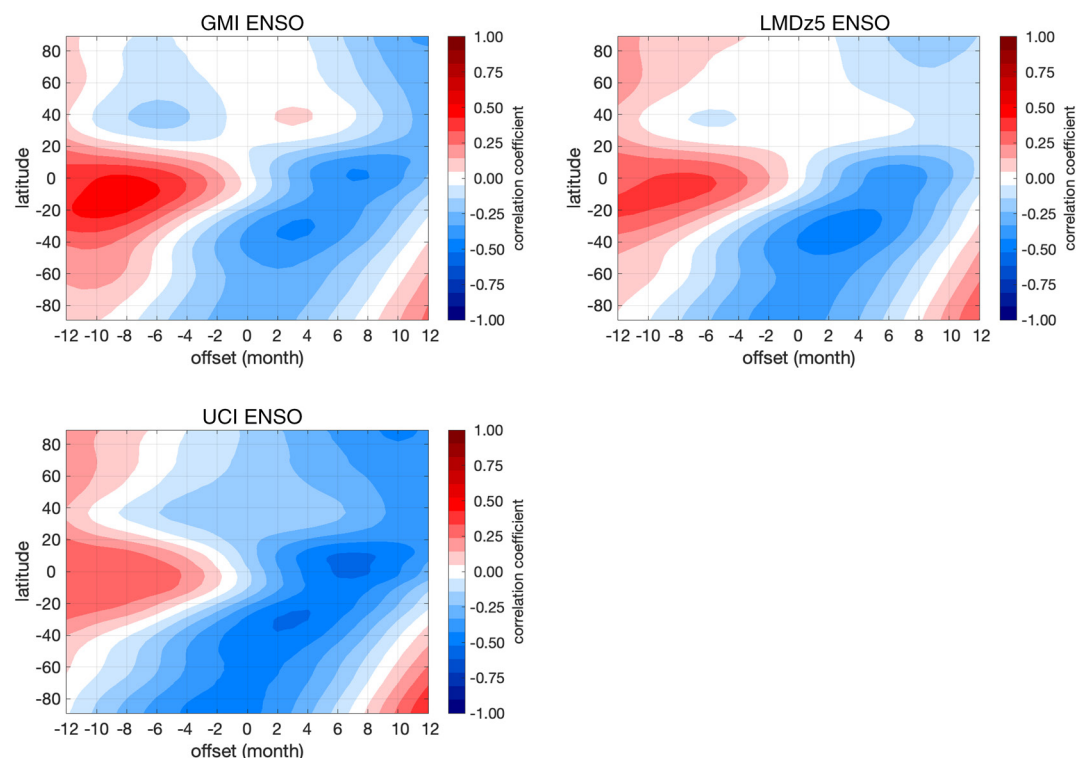
Figure 4. Correlation coefficients between surface N_2O residuals (NOAA N_2O minus modeled N2OX from Figure S2) and Niño 3.4 index at each latitude for years 2001–2016. The offset represents the lag between residuals and the Niño 3.4 index (i.e., −12 offset = N_2O residual$_{Jan2000}$ vs. the Niño Index$_{Jan2001}$). Before the residuals were calculated, the modeled surface variability was rescaled to match the RMS of the observed QBO signal in Figure 3. ENSO, El Niño-Southern Oscillation; N_2O, Nitrous oxide; NOAA, National Oceanic and Atmospheric Administration; QBO, Quasi-Biennial Oscillation.

with a lag of −2 to +4 months in the SH and occurring more weakly and 10 months later in the NH. All three models give the same basic pattern for ENSO-driven emissions.

4. Annual Surface Climatology

Nevison et al. (2004, Figure 1) noted that the annual cycle of N_2O at three remote sites was caused as much by the stratospheric influx of N_2O-depleted air as tropospheric transport of emissions. Thompson, Chevallier, et al. (2014a, Figure 8) compared the annual cycle of N_2O at seven remote sites in an 8-model intercomparison project that included surface emissions and model-calculated STE. Here, we construct a latitude-by-month annual cycle composite (in ppb) for each time series (observed N_2O, modeled N2OX and F11X) using a global rescaling factor so that the annual mean value is 320 ppb. These annual cycles, averaged over the years 2001–2016, are shown for all latitudes in supplementary Figure S5. The annual cycle in modeled F11X parallels that of N2OX (cc = 0.98 for GMI and 1.00 for UCI) but with twice the amplitude because of the shorter lifetime. While the modeled N2OX annual cycle is driven only by STE of N_2O-depleted air, the observed annual cycle of N_2O includes the signal of surface emissions and N-S transport of these emissions. In Figure 5, we compare the annual cycle in the NH and SH mid-latitudes (30°–90°) from observations and models. Our observed cycles, as expected, are similar to the mid- and high-latitude stations in Nevison et al. (2004) and Thompson, Chevallier, et al. (2014), with the notable exception of Trinidad Head, which does not match other NH stations.

First, it appears that the STE flux, both annual and QBO-related, creates only small N-S gradients, ranging from +0.3 ppb (UCI) to −0.2 ppb (LMDz5), and thus the observed gradient (+1.3 ppb) is driven predominantly by NH emissions. Second, the modeled NH annual amplitude looks much like the observations: the models peak to peak amplitude ranges from 0.51 to 0.75 with a June–August minimum; while the observed
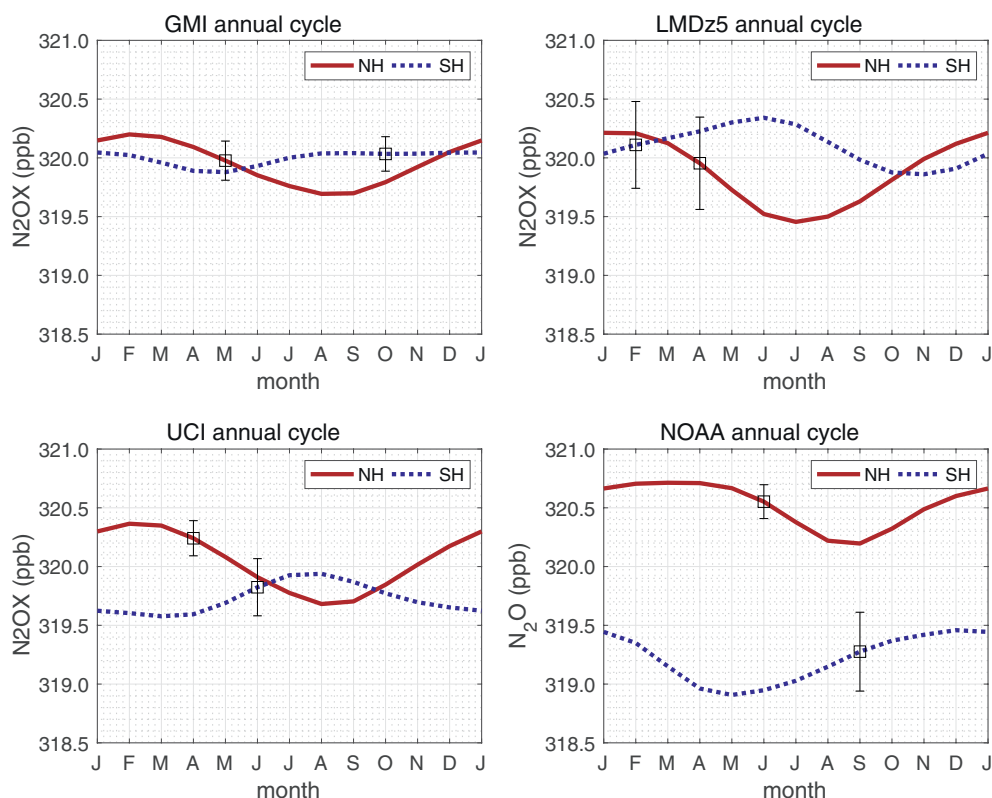
Figure 5. The annual cycle of surface N_2O/N2OX for the northern hemisphere (30°N–90°N; solid red line) and the southern hemisphere (30°–90°S; dashed blue line). Simulations (top panel and bottom left) are of N2OX (zero emissions), while the NOAA ESRL observations (bottom right) are of surface N_2O (with emissions). The 12-month running average of the global abundance for each data set was rescaled to 320 ppb. From there each month was averaged for the years 2001–2016 (i.e., all Januarys averaged, etc.). Vertical box-whiskers show the interannual peak-to-peak amplitude of the QBO in each hemisphere taken from Figure 3. ESRL, Earth System Research Laboratories; N_2O, Nitrous oxide; NOAA, National Oceanic and Atmospheric Administration; QBO, Quasi-Biennial Oscillation.

amplitude is ~0.50 ppb with an August–September minimum. Thus, the observed NH seasonality can be driven for the most part by the STE flux and not by seasonality of emissions or interhemispheric exchange. Third, for the SH, the amplitude is reduced and there is a range of phases between the models. It is interesting to note that the amplitude of the QBO in the mid-latitudes (box-whiskers on the annual cycles in Figure 5) can be as large or larger than the annual cycle and confounds a simple separation of the STE flux into annual and interannual cycles from observations.

With the model experiments conducted here, it is difficult to assess how STE flux competes with SH sources or interhemispheric exchange. We see agreement across the models in SH STE using QBO composites, but the annual cycles are discordant. Thompson, Chevallier, et al. (2014) recorded widespread disagreement of N_2O seasonality in the SH among six different models. We find here that the annual STE cycle in the SH is substantially different among three standard meteorological models (MERRA-2, ERA-Interim, ECM-WF-IFS), while in the NH it is essentially the same.

Nevison et al. (2004) showed the annual minimum of F11 occurred 1 month before that of N_2O in the SH (Cape Grim) due to the influence of N_2O sources. Since our model simulations do not have emissions or interhemispheric gradients driven by emissions, we find that the variations in F11 and N_2O are almost perfectly correlated (see discussion above and Table S2). A more detailed study of QBO- or STE-related diagnostics with these models or similar CTMs running with assimilated or forecast meteorology is needed, with a focus on the SH. Such a study should include correlated trace species (CF_2Cl_2 as in Nevison et al., 2004, Thompson, Chevallier, et al., 2014, and probably also O_3) and also isotopic studies that may be able to separate STE fluxes from oceanic emissions (McLinden et al., 2003). Since different N_2O isotopes have different sources

and stratospheric chemistry, inclusion of them in a future study will provide unique information about their transport (Nevison et al., 2005; Park et al., 2012).

5. Conclusions

This work expands the MLS N_2O lifetime record from 2005–2010 to 2005–2018, providing more than a decade of observations with which to test models. Despite small biases in total loss rates, we show that three chemistry-transport models using different meteorological fields can simulate the observed stratospheric variability of N_2O induced by the QBO. With this capability, we follow the stratospheric signals down to the surface across all latitudes. By comparing $CFCl_3$ (F11) and N_2O simulations, we find that the surface variability is driven almost entirely by dynamical variations in cross tropopause fluxes of air rather than by propagation of the variability in stratospheric loss.

At the surface, we are able to quantify the QBO fingerprint in N_2O, showing that, for the most part, the three models match the observed interannual variations in N_2O in both hemispheres despite the presence of emissions. The annual cycle in stratospheric influx (hard to validate with observations) is modeled to be only slightly larger than the QBO pattern. In the NH, the models without emissions can match much of the observations. In the SH, the models have a much weaker annual cycle and differ in phasing when compared to the observations, indicating possible influence of seasonal transport and SH sources. Thus, we have confidence based on three similar results, that the NH annual cycle in N_2O due to stratospheric influence is well determined in phase and amplitude. In addition, we have confidence that the north-south gradient in N_2O caused by the stratosphere is at most ±0.3 ppb, is much less than the observed interhemispheric gradient of ~1 ppb, which thus must be driven by emissions being larger in the NH than in the SH. Our results support this well-known feature of the N_2O budget derived from previous studies (Nevison et al., 2018; Thompson et al., 2019; Tian et al., 2020).

We investigate disruptions to the QBO, their impacts on N_2O loss, and the models' ability to capture these impacts. The models have trouble capturing the surface impact of anomalous QBOs which coincide with strong, but opposite ENSO events (La Niña (2010/11) versus El Niño (2015/16)), which further confounds the problem. Using the three CTMs in this study, we are able to remove the interannual variability at the surface driven by stratospheric chemistry and tracer transport, thus we produce clear signal of the anomalous emissions from the 2010 La Niña. These results highlight the capability of the QBO signal as a diagnostic metric with which to investigate model circulation and transport mechanisms on interannual time scales.

Another consequence of this study is the extremely tight correlation of the interannual surface variations in F11 with those of N_2O found in both models. With this relationship, it is possible to use the observed interannual N_2O variations to remove the stratospheric influence on F11 and deduce its changing emissions. Interannual variations in N_2O emissions will certainly disrupt this tight relationship, but based on the 2001–2016 record, these appear to be no larger than stratosphere-driven changes. This result indicates an improved constraint on F11 emissions is possible.

Data Availability Statement

The data and scripts used to produce the figures and tables in this work are accessible via the DRYAD repository with DOI https://doi.org/10.7280/D1JX0K

References

Baldwin, M. P., Gray, L. J., Dunkerton, T. J., Hamilton, K., Haynes, P. H., Holton, J. R., et al. (2001). The Quasi-Biennial Oscillation. *Reviews of Geophysics*, *39*(2), 179–229. https://doi.org/10.1029/1999RG000073

Ball, W. T., Rozanov, E. V., Alsing, J., Marsh, D. R., Tummon, F., Mortlock, D. J., et al. (2019). The Upper Stratospheric Solar Cycle Ozone Response. *Geophysical Research Letters*, *46*(3), 1831–1841. https://doi.org/10.1029/2018gl081501

Braesicke, P., Neu, J., Fioletov, V., Godin-Beekmann, S., Hubert, D., Petropavlovskikh, I., et al. (2018). Update on global ozone: Past, present, and future. In *Scientific assessment of ozone depletion* (pp. 230–231). .

Butchart, N. (2014). The Brewer-Dobson circulation. *Reviews of Geophysics*, *52*, 157–184. https://doi.org/10.1002/2013rg000448

Butler, J. H., Elkins, J. W., Thompson, T. M., & Egan, K. B. (1989). Tropospheric and dissolved N2O of the West Pacific and East Indian Oceans during the El Nino Southern Oscillation event of 1987. *Journal of Geophysical Research*, *94*(D12). https://doi.org/10.1029/jd094id12p14865

Ciais, P., Sabine, C., Bala, G., Bopp, L., Brovkin, V., Canadell, J., et al. (2013). The physical science basis. Contribution of working group I to the fifth assessment report of the intergovernmental panel on climate change. *Change, IPCC Climate*, 465–570. https://doi.org/10.1017/CBO9781107415324.015

Cline, J. D., Wisegarver, D. P., & Kelly-Hansen, K. (1987). Nitrous oxide and vertical mixing in the equatorial Pacific during the 1982-1983 El Niño. *Deep-Sea Research Part A. Oceanographic Research Papers*, *34*(5–6), 857–873. https://doi.org/10.1016/0198-0149(87)90041-0

Corazza, M., Bergamaschi, P., Vermeulen, A. T., Aalto, T., Haszpra, L., Meinhardt, F., et al. (2010). Inverse modeling of European N 2 O emissions: Assimilating observations from different networks. *Atmospheric Chemistry and Physics Discussions*, *10*(11), 26319–26359. https://doi.org/10.5194/acpd-10-26319-2010

Coy, L., Newman, P. A., Pawson, S., & Lait, L. R. (2017). Dynamics of the disrupted 2015/16 quasi-biennial oscillation. *Journal of Climate*, *30*(15), 5661–5674. https://doi.org/10.1175/jcli-d-16-0663.1

Coy, L., Wargan, K., Molod, A. M., McCarty, W. R., & Pawson, S. (2016). Structure and dynamics of the Quasi-biennial oscillation in MER-RA-2. *Journal of Climate*, *29*(14), 5339–5354. https://doi.org/10.1175/jcli-d-15-0809.1

Dlugokencky, E. J., Crotwell, A. M., Mund, J. W., Crotwell, M. J., & Thoning, K. W. (2019). *Atmospheric nitrous oxide dry air mole fractions from the NOAA ESRL Carbon cycle cooperative global air sampling network. 1997–2018, Version: 2019-07*. https://doi.org/10.15138/53g1-x417

Douglass, A. R., Strahan, S. E., Oman, L. D., & Stolarski, R. S. (2017). Multi-decadal records of stratospheric composition and their relationship to stratospheric circulation change. *Atmospheric Chemistry and Physics*, *17*(19), 12081–12096. https://doi.org/10.5194/acp-17-12081-2017

Erisman, J. W., Galloway, J. N., Seitzinger, S., Bleeker, A., Dise, N. B., Roxana Petrescu, A. M., et al. (2013). Consequences of human modification of the global nitrogen cycle. *Philosophical Transactions of the Royal Society B: Biological Sciences*, *368*(1621). https://doi.org/10.1098/rstb.2013.0116

Fowler, D., Steadman, C. E., Stevenson, D., Coyle, M., Rees, R. M., Skiba, U. M., et al. (2015). Effects of global change during the 21st century on the nitrogen cycle. *Atmospheric Chemistry and Physics*, *15*(24), 13849–13893. https://doi.org/10.5194/acp-15-13849-2015

Froidevaux, L., Anderson, J., Wang, H.-J., Fuller, R. A., Schwartz, M. J., Santee, M. L., et al. (2015). Global OZone Chemistry And Related trace gas Data records for the Stratosphere (GOZCARDS): Methodology and sample results with a focus on HCl, H2O, and O3. *Atmospheric Chemistry and Physics*, *15*(18), 10471–10507. https://doi.org/10.5194/acp-15-10471-2015

Froidevaux, L., Kinnison, D. E., Wang, R., Anderson, J., & Fuller, R. A. (2019). Evaluation of CESM1 (WACCM) free-running and specified dynamics atmospheric composition simulations using global multispecies satellite data records. *Atmospheric Chemistry and Physics*, *19*(7), 4783–4821. https://doi.org/10.5194/acp-19-4783-2019

Fu, Q., Solomon, S., Pahlavan, H. A., & Lin, P. (2019). *Observed changes in Brewer – Dobson circulation*.

Gray, L. J., Beer, J., Geller, M., Haigh, J. D., Lockwood, M., Matthes, K., et al. (2010). Solar influences on climate. *Reviews of Geophysics*, *48*(4). https://doi.org/10.1029/2009rg000282

Hall, B. D., Dutton, G. S., & Elkins, J. W. (2007). The NOAA nitrous oxide standard scale for atmospheric observations. *Journal of Geophysical Research*, *112*(9), 1–9. https://doi.org/10.1029/2006jd007954

Hamilton, K., & Fan, S.-M. (2000). Effects of the stratospheric quasi-biennial oscillation on long-lived greenhouse gases in the troposphere. *Journal of Geophysical Research*, *105*(D16), 20581–20587. https://doi.org/10.1029/2000jd900331

Hood, L. L. (2004). Effects of solar UV variability on the stratosphere. *Geophysical Monograph Series*, *141*, 283–303. https://doi.org/10.1029/141gm20

Hsu, J., & Prather, M. J. (2009). Stratospheric variability and tropospheric ozone. *Journal of Geophysical Research*, *114*(6), 1–15. https://doi.org/10.1029/2008jd010942

Hsu, J., & Prather, M. J. (2010). Global long-lived chemical modes excited in a 3-D chemistry transport model: Stratospheric N2O, NOy, O3 and CH 4 chemistry. *Geophysical Research Letters*, *37*(7), 1–5. https://doi.org/10.1029/2009gl042243

Ji, Q., Altabet, M. A., Bange, H. W., Graco, M. I., Ma, X., Arévalo-Martínez, D. L., & Grundle, D. S. (2019). Investigating the effect of El Niño on nitrous oxide distribution in the eastern tropical South Pacific. *Biogeosciences*, *16*(9), 2079–2093. https://doi.org/10.5194/bg-16-2079-2019

Livesey, N. J., Read, W. G., Wagner, P. A., Froidevaux, L., Lambert, A., Manney, G. L., et al. (2018). *Earth observing system (EOS) Aura Microwave Limb Sounder (MLS) version 4.2x level 2 data quality and description document*.

Livesey, N. J., Read, W. G., Wagner, P. A., Froidevaux, L., Santee, M. L., Schwartz, M. J., et al. (2020). *Earth observing system (EOS) Aura Microwave Limb Sounder (MLS) version 5.0x level 2 and 3 data quality and description document*. Retrieved from https://mls.jpl.nasa.gov/data/datadocs.php

Mahlman, J. D., Levy, H., & Moxim, W. J. (1986). Three-dimensional simulations of stratospheric N2O: Predictions for other trace constituents. *Journal of Geophysical Research*, *91*(D2), 2687–2707. https://doi.org/10.1029/jd091id02p02687

Manney, G. L., Hegglin, M. I., Lawrence, Z. D., Wargan, K., Millán, L. F., Schwartz, M. J., et al. (2017). Reanalysis comparisons of upper tropospheric-lower stratospheric jets and multiple tropopauses. *Atmospheric Chemistry and Physics*, *17*(18), 11541–11566. https://doi.org/10.5194/acp-17-11541-2017

McLinden, C. A., Prather, M. J., & Johnson, M. S. (2003). Global modeling of the isotopic analogs of N2O: Stratospheric distributions, budgets, and the 17O-18O mass-independent anomaly. *Journal of Geophysical Research*, *108*(8), 1–15. https://doi.org/10.1029/2002jd002560

Montzka, S. A., Dutton, G. S., Yu, P., Ray, E., Robert, W., Daniel, J. S., et al. (2018). An unexpected and persistent increase in global emissions of ozone-depleting CFC-11. *Nature*, *557*(7705), 413–417. https://doi.org/10.1038/s41586-018-0106-2

Nevison, C., Andrews, A., Thoning, K., Dlugokencky, E., Sweeney, C., Miller, S., et al. (2018). Nitrous oxide emissions estimated with the carbontracker-lagrange North American regional inversion framework. *Global Biogeochemical Cycles*, *32*(3), 463–485. https://doi.org/10.1002/2017gb005759

Nevison, C. D., Dlugokencky, E., Dutton, G., Elkins, J. W., Fraser, P., Hall, B., et al. (2011). Exploring causes of interannual variability in the seasonal cycles of tropospheric nitrous oxide. *Atmospheric Chemistry and Physics*, *11*(8), 3713–3730. https://doi.org/10.5194/acp-11-3713-2011

Nevison, C. D., Keeling, R. F., Weiss, R. F., Popp, B. N., Jin, X., Fraser, P. J., et al. (2005). Southern Ocean ventilation inferred from seasonal cycles of atmospheric N2O and O2/N2 at Cape Grim, Tasmania. *Tellus B: Chemical and Physical Meteorology*, *57*(3), 218–229. https://doi.org/10.3402/tellusb.v57i3.16533

Nevison, C. D., Kinnison, D. E., & Weiss, R. F. (2004). Stratospheric influences on the tropospheric seasonal cycles of nitrous oxide and chlorofluorocarbons. *Geophysical Research Letters*, *31*(20), 1–5. https://doi.org/10.1029/2004gl020398

Nevison, C. D., Mahowald, N. M., Weiss, R. F., & Prinn, R. G. (2007). Interannual and seasonal variability in atmospheric N2O. *Global Biogeochemical Cycles*, *21*(3), 1–13. https://doi.org/10.1029/2006gb002755

Newman, P. (2020). NASA, G. *The quasi-biennial oscillation (QBO)*. Retrieved from https://acd-ext.gsfc.nasa.gov/Data_services/met/qbo/qbo.html

Newman, P. A., Coy, L., Pawson, S., & Lait, L. R. (2016). The anomalous change in the QBO in 2015–2016. *Geophysical Research Letters*, *43*(16), 8791–8797. https://doi.org/10.1002/2016gl070373

Osprey, S. M., Butchart, N., Knight, J. R., Scaife, A. A., Hamilton, K., Anstey, J. A., et al. (2016). An unexpected disruption of the atmospheric quasi-biennial oscillation. *Science*, *353*(6306), 1424–1427. https://doi.org/10.1126/science.aah4156

Park, S., Croteau, P., Boering, K. A., Etheridge, D. M., Ferretti, D., Fraser, P. J., et al. (2012). Trends and seasonal cycles in the isotopic composition of nitrous oxide since 1940. *Nature Geoscience*, *5*(4), 261–265. https://doi.org/10.1038/ngeo1421

Prather, M. J. (1998). Time Scales in Atmospheric Chemistry: Coupled Perturbations to N2O, NOy, and O3. *Science*, *279*(5355), 1339–1341. https://doi.org/10.1126/science.279.5355.1339

Prather, M. J., Holmes, C. D., & Hsu, J. (2012). Reactive greenhouse gas scenarios: Systematic exploration of uncertainties and the role of atmospheric chemistry. *Geophysical Research Letters*, *39*(9), 6–10. https://doi.org/10.1029/2012gl051440

Prather, M. J., Hsu, J., Deluca, N. M., Jackman, C. H., Oman, L. D., Douglass, A. R., et al. (2015). Measuring and modeling the lifetime of nitrous oxide including its variability. *Journal of Geophysical Research: Atmosphere*, 1–13.

Prather, M. J., Zhu, X., Flynn, C. M., Strode, S. A., Rodriguez, J. M., Steenrod, S. D., et al. (2017). Global atmospheric chemistry – Which air matters. *Atmospheric Chemistry and Physics*, *17*(14), 9081–9102. https://doi.org/10.5194/acp-17-9081-2017

Ray, E. A., Portmann, R. W., Yu, P., Daniel, J., Montzka, S. A., Dutton, G. S., et al. (2020). The influence of the stratospheric Quasi-Biennial Oscillation on trace gas levels at the Earth's surface. *Nature Geoscience*, *13*(1), 22–27. https://doi.org/10.1038/s41561-019-0507-3

Remaud, M., Chevallier, F., Cozic, A., Lin, X., & Bousquet, P. (2018). On the impact of recent developments of the LMDz atmospheric general circulation model on the simulation of CO2 transport. *Geoscientific Model Development*, *11*(11), 4489–4513. https://doi.org/10.5194/gmd-11-4489-2018

Rigby, M., Park, S., Saito, T., Western, L. M., Redington, A. L., Fang, X., et al. (2019). Increase in CFC-11 emissions from eastern China based on atmospheric observations. *Nature*, *569*(7757), 546–550. https://doi.org/10.1038/s41586-019-1193-4

Serva, F., Cagnazzo, C., Christiansen, B., & Yang, S. (2020). The influence of ENSO events on the stratospheric QBO in a multi-model ensemble. *Climate Dynamics*, *54*(3–4), 2561–2575. https://doi.org/10.1007/s00382-020-05131-7

Stauffer, R. M., Thompson, A. M., Oman, L. D., & Strahan, S. E. (2019). The Effects of a 1998 Observing System Change on MERRA-2-Based Ozone Profile Simulations. *Journal of Geophysical Research: Atmosphere*, *124*(13), 7429–7441. https://doi.org/10.1029/2019JD030257

Strahan, S. E., Douglass, A. R., & Steenrod, S. D. (2016). Chemical and dynamical impacts of stratospheric sudden warmings on Arctic ozone variability. *Journal of Geophysical Research: Atmosphere*, *175*(4449), 238. https://doi.org/10.1038/175238c0

Strahan, S. E., Oman, L. D., Douglass, A. R., & Coy, L. (2015). Modulation of Antarctic vortex composition by the quasi-biennial oscillation. *Geophysical Research Letters*, *42*(10), 4216–4223. https://doi.org/10.1002/2015gl063759

Thompson, R. L., Bousquet, P., Chevallier, F., Rayner, P. J., & Ciais, P. (2011). Impact of the atmospheric sink and vertical mixing on nitrous oxide fluxes estimated using inversion methods. *Journal of Geophysical Research*, *116*(17), 1–14. https://doi.org/10.1029/2011jd015815

Thompson, R. L., Chevallier, F., Crotwell, A. M., Dutton, G., Langenfelds, R. L., Prinn, R. G., et al. (2014). Nitrous oxide emissions 1999 to 2009 from a global atmospheric inversion. *Atmospheric Chemistry and Physics*, *14*(4), 1801–1817. https://doi.org/10.5194/acp-14-1801-2014

Thompson, R. L., Ishijima, K., Saikawa, E., Corazza, M., Karstens, U., Patra, P. K., et al. (2014). TransCom N2O model inter-comparison – Part 2: Atmospheric inversion estimates of N2O emissions. *Atmospheric Chemistry and Physics*, *14*(12), 6177–6194. https://doi.org/10.5194/acp-14-6177-2014

Thompson, R. L., Lassaletta, L., Patra, P. K., Wilson, C., Wells, K. C., Gressent, A., et al. (2019). Acceleration of global N2O emissions seen from two decades of atmospheric inversion. *Nature Climate Change*, *9*(12), 993–998. https://doi.org/10.1038/s41558-019-0613-7

Thompson, R. L., Patra, P. K., Ishijima, K., Saikawa, E., Corazza, M., Karstens, U., et al. (2014). TransCom N2O model inter-comparison – Part 1: Assessing the influence of transport and surface fluxes on tropospheric N2O variability. *Atmospheric Chemistry and Physics*, *14*(8), 4349–4368. https://doi.org/10.5194/acp-14-4349-2014

Tian, H., Xu, R., Canadell, J. G., Thompson, R. L., Winiwarter, W., Suntharalingam, P., et al. (2020). A comprehensive quantification of global nitrous oxide sources and sinks. *Nature*, *586*(7828), 248–256. https://doi.org/10.1038/s41586-020-2780-0

Tian, H., Yang, J., Lu, C., Xu, R., Canadell, J. G., Jackson, R. B., et al. (2018). The global N2O model intercomparison project. *Bulletin of the American Meteorological Society*, *99*(6), 1231–1251. https://doi.org/10.1175/bams-d-17-0212.1

Volk, C. M., Elkins, J. W., Fahey, D. W., Dutton, G. S., Gilligan, J. M., Loewenstein, M., et al. (1997). Evaluation of source gas lifetimes from stratospheric observations. *Journal of Geophysical Research*, *102*(21), 25543–25564. https://doi.org/10.1029/97jd02215